Sputtering yields of Ru, Mo, and Si under low energy Ar^+ bombardment

Shiou-Min Wu,[a] Robbert van de Kruijs, Erwin Zoethout, and Fred Bijkerk[b]
FOM Institute for Plasma Physics Rijnhuizen, P.O. Box 1207, 3430 BE Nieuwegein, The Netherlands

(Received 16 March 2009; accepted 10 May 2009; published online 4 September 2009)

Ion sputtering yields for Ru, Mo, and Si under Ar^+ ion bombardment in the near-threshold energy range have been studied using an *in situ* weight-loss method with a Kaufman ion source, Faraday cup, and quartz crystal microbalance. The results are compared to theoretical models. The accuracy of the *in situ* weight-loss method was verified by thickness-decrease measurements using grazing incidence x-ray reflectometry, and results from both methods are in good agreement. These results provide accurate data sets for theoretical modeling in the near-threshold sputter regime and are of relevance for (optical) surfaces exposed to plasmas, as, for instance, in extreme ultraviolet photolithography. © *2009 American Institute of Physics*. [doi:10.1063/1.3149777]

I. INTRODUCTION

The lifetime of multilayer coated reflective optics is one of the most important issues for the next generation of photolithography equipment utilizing extreme ultraviolet (EUV) wavelengths.[1] This is particularly crucial and challenging in the case of so-called collector optics, which directly face a high-power plasma light source to capture the EUV light. Srivastava *et al.*[2] recently reported measurements and calculations of the collector lifetime relevant to erosion of the topmost surface by bombardment with energetic Xe or Sn debris from EUV light sources. Erosion of the collector surface can also be caused by the secondary plasma produced by the interaction of EUV light and buffer gasses used in the EUV source. Recently, van der Velden *et al.*[3,4] and Wieggers *et al.*[5] extensively modeled this secondary plasma induced damage using an analytical technique and particle-in-cell Monte Carlo simulations. So far, these theoretical predictions are lacking recent and accurate sputtering yield data for low energy ion (<100 eV) bombardment of thin films.

Sputtering is the erosion of a solid surface by energetic particle bombardment.[6] Sputtering yield is defined as average number of ejected target atoms per incident ion. For a simple physical sputtering system, the yield is described in terms of $Y(E,\theta,M_1,Z_1,M_2,Z_2)$, which is dependent on the incident ion energy E, incident angle θ relative to the target surface normal, and the mass M and atomic number Z with indices 1 and 2 standing for incident ions and target atoms, respectively. The yield is generally described based on the effects of mass ratios $A \equiv M_2/M_1$, surface binding energies U_s, and the nuclear stopping power $S_n(E)$.[7–9] Analytical models of the sputtering yield at normal incidence ($\theta=0$), including models of Bohdansky[7] and Yamamura and Tawara,[8] are used to describe the sputtering experiments presented in this paper, and a brief description will be given in Sec. III.

At ion energies near the sputter threshold regime it is challenging to accurately determine sputtering yields because of the low yields and the difficulty in preparation of a high flux and monoenergetic low energy ion beam. Previous measurements of sputtering yields of metals for Ar^+ and Ne^+ ions with energies from 50 to 600 eV were done by Laegreid and Wehner[10] in 1961, though not for near-threshold energies. In addition, the yields were determined by *ex situ* weight-loss measurements of spherical targets immersed like large negative Langmuir probes in a dense low-pressure plasma. In this paper, we discuss sputtering yield experiments on Ru, Mo, and Si, materials commonly considered for use in optical coatings for the EUV wavelength range.[11,12] We present *in situ* weight-loss measurements in an ultrahigh vacuum system, resulting in accurate sputtering yield determination notably for low to near-threshold sputter energies.

II. EXPERIMENT

In situ weight-loss measurements were carried out to measure the sputtering yields using a Kaufman type ion source, a retarding field analyzer/Faraday cup (RFA/FC), and a quartz crystal microbalance (QCM). Comparing to previous similar experiments in literature,[13] the broad and homogeneous ion beam used in this study makes simultaneous measurements of the ion flux and the weight loss possible.

The ion source used in this study is a three-grid broad beam (15 cm diameter) ion source with a thermionic cathode filament and permanent magnet confinement elements. The flow rate of Ar was 10 SCCM (SCCM denotes standard cubic centimeter per minute at STP), and the chamber pressure was 8×10^{-5} mbar (with less than 1% residual gases) during the ion exposure. The double ionization energy of Ar atom is 43.4 eV, and the discharge potential was set to be 35 V to prevent formation of doubly charged ions. The three-grid system, composed by screen, accelerator and ground grids, extracts the ions and serves as an ion lens. The screen potential is floating, while the accelerator potential is set to extract ions. In our ion source, the aperture size of the accelerator grid is designed to be less than the aperture size of the screen grid to enhance the ion flux. In this study, the ion flux was maximized by tuning the accelerator potential, and the ion current to the accelerator was minimized (<10 mA) to re-

[a]Author to whom correspondence should be addressed. Electronic mail: m.wu@rijnhuizen.
[b]Also at MESA+ Institute for Nanotechnology, University of Twente, Enschede, The Netherlands.

duce sputtering of the accelerator grid material. The RFA/FC (CEA3, CCR GmbH) and the QCM (XTM/2, Inficon) were mounted 6.5 cm in front of the Kaufman ion source at a 4.5 cm radius off the ion beam center axis to ensure equal ion doses on both devices.

The sputter targets consisted of 100 nm thin films of Ru, Mo, or Si precoated on the QCM using physical vapor deposition (PVD) with electron beam evaporation technology. The RFA/FC consists of a front cover with an aperture of 0.5 mm diameter, a retarding field electrode for electron repulsion, and a retarding field cup electrode for ion repulsion. During the experiment, the RFA/FC ran in two modes: one in which the RFA mode was employed before and after each experiment to measure the ion energy distributions and another in which the FC mode was used to monitor the ion flux for the *in situ* sputtering yield measurement (without ion retarding field). The ion flux and weight loss were simultaneously measured during sputtering using FC and QCM, respectively, and the control and signal acquisition was done using LABVIEW software (National Instruments) in a personal computer. Further pre- and postsputtering analyses were performed using angle resolved x-ray photoelectron spectroscopy (Theta probe AR-XPS, Thermal Scientific) and scanning electron microscopy (SEM) to check the chemical components of the coated layer as well as the amount of implanted Ar^+ ion and the topography of the quartz, respectively.

In order to confirm the accuracy of the weight-loss measurements, a separate experiment was carried out where a sample with a ~10 nm Ru layer was added near the RFA/FC and QCM and in the same radius off the center of ion beam axis. The Ru layer was PVD coated on a superpolished Si wafer (25×25 mm^2, rms<0.2 Å, and native oxide of ~2 nm SiO_2). The thickness change resulting from the sputter experiment was obtained *in situ* using the RFA/FC and QCM and *ex situ* by means of grazing incidence x-ray reflectometry (GIXR) using a Philips X'Pert double crystal x-ray diffractometer at Cu $K\alpha$ line radiation (0.154 nm). The software package IMD (Ref. 14) was used to fit reflectivity simulations to the experimental data, primarily yielding Ru layer thickness, density, and roughness.

III. ANALYTICAL EXPRESSIONS

Empirical expressions derived by Bohdansky[7] and Yamamura and Tawara[8] were used to interpret the experimental results obtained in this study. These analytical expressions of sputtering yield at normal incidence ($\theta=0$) are based on Sigmund's results: $Y(E)=(0.042\alpha/U_s)S_n(E)$,[15] in which the sputtering yield $Y(E)$ is inversely proportional to the surface binding energy U_s (generally approximated by the heat of sublimation, in eV) and proportional to the deposited energy at the surface. The deposited energy is proportional to $\alpha S_n(E)$ in which $S_n(E)$ is the nuclear stopping cross section and $\alpha(M_2/M_1)$ is a best-fit parameter. Sigmund's equation however generally fails to describe experimental data sputtering yields either in the lower incident energy range or for light incident ions. To solve these problems, Bohdansky proposed a universal relation as follows:[7]

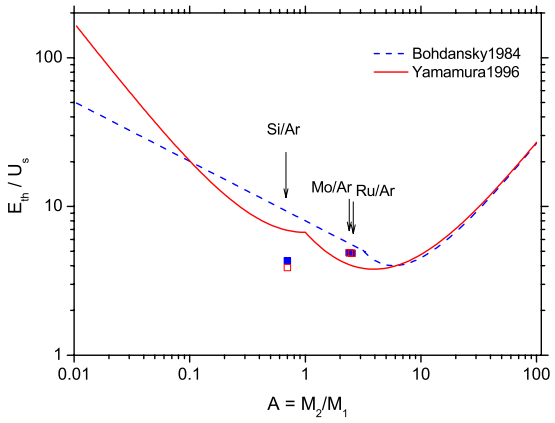

FIG. 1. (Color online) The empirical curves of E_{th}/U_s as functions of mass ratios $A\equiv M_2/M_1$ used in Bohdansky's model (Ref. 7) [Eq. (1)] and Yamamura and Tawara's model (Ref. 8) [Eq. (2)]. The solid and open squares are the new-fit parameters determined from the current study (see Table II).

$$Y(E)=0.042\frac{(R_P/R)\alpha}{U_s}S_n^{\mathrm{TF}}(E)\left[1-\left(\frac{E_{\mathrm{th}}}{E}\right)^{2/3}\right]\left(1-\frac{E_{\mathrm{th}}}{E}\right)^2. \tag{1}$$

In this equation, the sputtering yield in lower incident energy range (near sputtering threshold energy E_{th}) is corrected by two factors: one, the *effectively* deposited energy, which is $\alpha S_n(E)$ multiplied by a factor of $1-(E_{\mathrm{th}}/E)^{2/3}$, and the other, the momentum distribution of the recoiling target atoms by a factor of $(1-E_{\mathrm{th}}/E)^2$. The sputtering yield for light projectile ions is corrected by a factor of R_P/R in which R_p is the projected range of the average path length R. Nuclear stopping power for the Thomas–Fermi potential $S_n^{\mathrm{TF}}(E)$ is used. In order to improve the accuracy of the universal expression, Yamamura and Tawara[8] derived a new universal equation as follows:

$$Y(E)=0.042\frac{Q\alpha'}{U_s}\frac{S_n^{\mathrm{TF}}(E)}{1+\Gamma k_e\varepsilon^{0.3}}\left(1-\sqrt{\frac{E_{\mathrm{th}}}{E}}\right)^s, \tag{2}$$

where k_e is the Lindhard electronic stopping coefficient, ε is the reduced energy, and $\Gamma=W/[1+(M_1/7)^3]$ is a dimensionless factor. $Q(Z_2)$, typically a factor around unity, comes from the energy loss of the sputtered particles between the point of origin and the surface. $W(Z_2)$ may reflect the electronic stopping power (typically $W=0.35U_s$), and $s(Z_2)$ is used to fine-tune the sputtering yield in the near-threshold range (typically $s=2.5$). The parameters $E_{\mathrm{th}}/U_s(M_2/M_1)$ used in Yamamura–Tawara's and Bohdansky's equations are plotted in Fig. 1, and an evaluation of both equations to describe experimental sputtering yields in the near-threshold energy regime will be presented in Sec. V.

IV. RESULTS

Before and after each sputtering experiment, the ion energy distributions of the Kaufman ion source were measured using the RFA and fitted by Gaussian distributions. For the range of energies used in the current studies, the average ion beam energy agrees well with the Kaufman anode potential

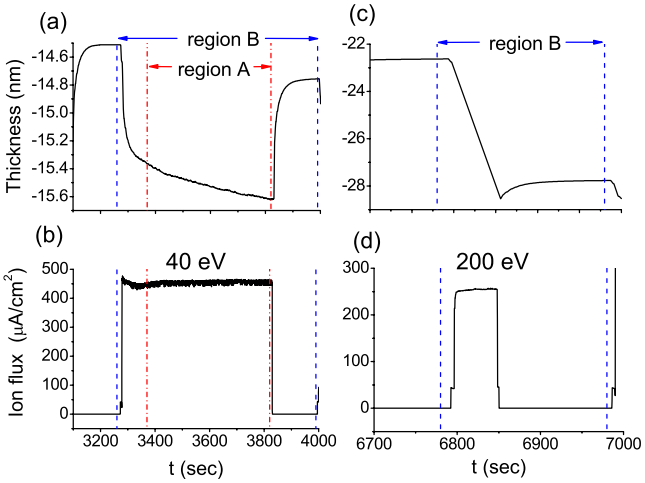

FIG. 2. (Color online) Two representative sets of *in situ* signals ($Ar^+ \rightarrow Ru$) of thickness and ion flux measured using QCM (top panels) and FC (bottom panels), respectively. The ion energies for [(a) and (b)] left panels and [(c) and (d)] right panels are 40 and 200 eV, respectively. Regions A and B are selected for extracting the sputtering yields Y_1 and Y_2, respectively.

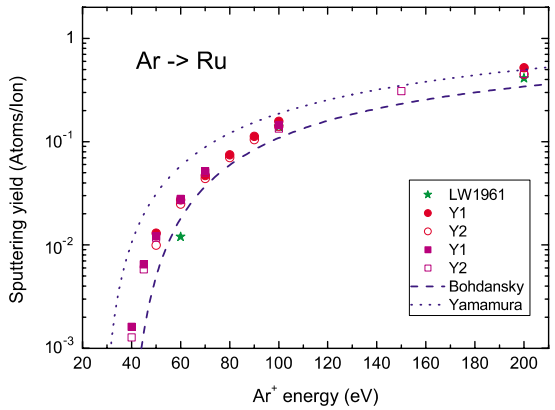

FIG. 3. (Color online) Comparison of the experimental near-threshold ($Ar^+ \rightarrow Ru$) sputtering yield to empirical curves. The experimental data points Y_1 and Y_2 are extracted by two different methods due to the QCM distortion effects (see Fig. 2), while circles and squares represent two data sets that resulted from different QCMs. The empirical curves are calculated using the original parameters described in Refs. 7 and 8.

(within 1 V), and the ion beam energy spread was typically 6 eV (Gaussian widths), sufficiently small compared to the energies used in this study.

As an example, two representative data sets of *in situ* sputtering measurements on a 100 nm Ru layer are shown in Fig. 2. The thickness of the coated layer on top of the quartz during sputtering was calculated using the Sauerbrey equation[16]

$$d = \frac{N_Q \rho_Q}{\pi \rho f Z} \tan^{-1}\left[Z \tan\left(\pi \frac{f_0 - f}{f_0} \right) \right] \times 0.1 \text{ nm}, \quad (3)$$

where N_Q is the frequency constant for an AT-cut quartz crystal (1.668×10^{13} Hz Å), ρ_Q is the density of quartz (2.648 g/cm^3), ρ is the density of the deposited material, f is the frequency of the loaded crystal, f_0 is the frequency of the unloaded crystal (6 MHz), and Z is the acoustic impedance ratio. Due to external influences, such as ion impact and QCM temperature, the thickness signal is distorted directly after switching the ion gun on and off. The distortion is clearly larger for lower energy ions due to the lower sputtering rates [see also Fig. 2(a)]. Due to these artifacts, two methods were chosen to extract the sputtering yields. In the first case, the sputtering yield Y_1 was calculated using the constant thickness change rate and ion flux in region A, indicated in Fig. 2. In the second case, the sputtering yield Y_2 was calculated using the total thickness change and total ion fluence in region B, indicated in Fig. 2. The distortion effect is relatively less significant for higher ion energies because the sputtering yields increase nonlinearly near the threshold energy. For higher energies such as 200 eV, as shown in Fig. 2(c), the first method is not used because a steady rate of the quartz frequency change could not be reached in timeframe of the experiment due to the high sputtering rate and limited amount of coated Ru on the QCM.

The maximum ion flux decreased when the ion energy decreased; e.g., for an ion energy of 40 eV, the maximum ion flux was limited to 0.45 mA cm^{-2} (i.e., 2.8×10^{15} ions cm^{-2} s^{-1}) [see also Fig. 2(b)]. To investigate the dependence of sputtering yield on ion flux, several different ion fluxes were used, and the resulting sputtering yields were consistent, showing no significant flux dependence. For each experimental run, different ion energies were used in an arbitrary sequence to eliminate systematic errors. The same energy was repeated several times and the results were reproducible, indicating that the effects of surface modification, temperature difference, ion implantation, etc. were negligible. The sputtering yield results are averaged and plotted in Fig. 3. We can see that the yields Y_1 and Y_2 extracted by the above two methods are consistent. Two data sets, circles and squares, which resulted from different QCMs, confirm the reproducibility of this method. Sputtering experiments were repeated for Mo and Si, and the results are shown in Fig. 4 and listed in Table I. More discussions on the sputtering yield results will be given in the following section.

An XPS analysis of the Ru thin film shows approximately 1 nm of ruthenium oxide on top of the Ru layer, which was removed by ion sputtering before initiating the sputtering yield measurements. No Ar was observed by XPS analysis after sputtering experiments, which shows that less than 1% of Ar was implanted during sputtering. The roughness of the QCM surface was of the order of a micrometer, and the SEM images show that the roughness did not change before and after the ion exposure.

To investigate the effect of surface roughness and validate the sputtering yield data obtained using a QCM, additional experiments were carried out on Ru thin films. Two superpolished Si substrates with a 10 nm coated Ru layer on top were exposed to 50 eV ions for 30 min and 200 eV for 1 min, respectively, while simultaneously exposing the RFA/FC and QCM. Figure 5 shows the Cu $K\alpha$ GIXR spectra of the Ru film before and after 50 eV Ar^+ ion irradiation, as well as model simulations performed using IMD. The analysis shows that the thickness of the Ru layer decreased from 11.6 to 8.4 and 6.2 nm after exposure to energies of 50 and 200 eV, respectively. The density parameter of the Ru film before and after low energy ion bombardment was 11.2 ± 0.2 g/cm^3, slightly less than the bulk value of

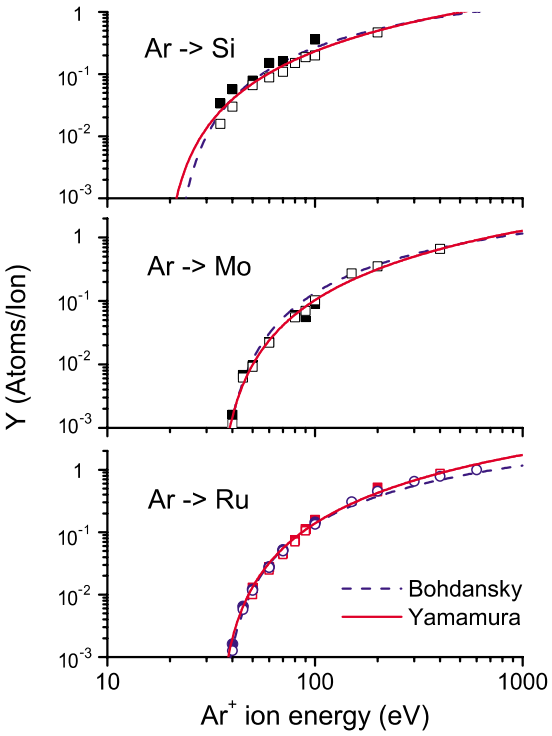

FIG. 4. (Color online) Sputtering yields of Si, Mo, and Ru under low energy Ar^+ ion irradiation. See the caption of Fig. 3 for the description of the experimental data points. The calculated curves are fitted using Bohdansky's and Yamamura and Tawara's expressions [Eqs. (1) and (2), respectively] with the new-fit parameters listed in Table II.

12.3 g/cm^3, and is typical for polycrystalline thin films deposited using low adatom energy deposition techniques. The Ru surface became smoother (roughness parameter reduces from 8.5 to 5 and 3 Å, respectively) after ion bombardment at 50 and 200 eV. From the thickness change and film density, the amount of sputtered atoms was determined, providing an alternative determination of sputtering yield. The results were in good agreement with those obtained using *in situ* weight-loss measurements. These data further confirm the accuracy of the results from the *in situ* QCM signals as

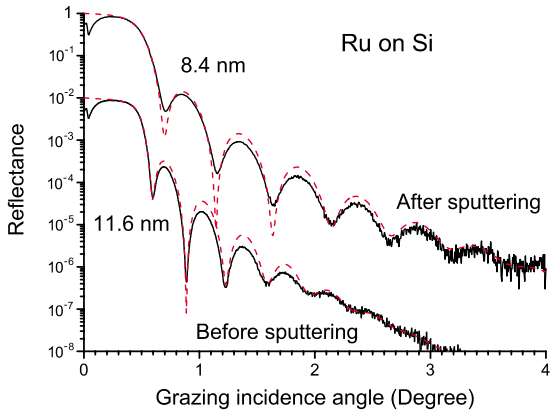

FIG. 5. (Color online) GIXR spectra from a thin Ru film taken before and after Ar^+ ion sputtering at 50 eV. The solid and dashed curves are the experimental data and simulations, respectively. The curves "before sputtering" are offset by a factor of 0.01 for display purposes.

well as show that the sputtering yields on a film deposited on a rough QCM surface are comparable with those of a film deposited on a smooth Si wafer.

V. DISCUSSION

To describe the near-threshold sputtering yields obtained in this work, we compare curves calculated from the expressions of Bohdansky and Yamamura–Tawara with our experimental data. Figure 3 shows that our experimental sputtering yields near-threshold energies for Ru are between the two predictions such that Bohdansky's formula predicts a too high threshold energy, while Yamamura's formula predicts a too low threshold energy. It should be noted that the formulas used in both calculations are empirical and threshold energies are based on data taken at considerably higher energies (typically $\gg$100 eV). Similar discrepancies between experimental data and model simulations based on these two formulas were observed for Mo and Si.

To improve the agreement between the theoretical models and the near-threshold data presented here, fits to the data

TABLE I. Sputtering yields for Si, Mo, and Ru under Ar^+ ion bombardment. See text for more details regarding the two different methods of extracting sputtering yields Y_1 and Y_2.

E	Si		Mo		Ru			
(eV)	Y_1	Y_2	Y_1	Y_2	Y_1	Y_2	Y_1	Y_2
35	0.034	0.016						
40	0.058	0.030	0.0016	0.0011			0.0016	0.0013
45			0.0069	0.0062			0.0065	0.0058
50	0.079	0.067	0.0096	0.0091	0.013	0.010	0.012	0.012
60	0.15	0.089	0.023	0.022	0.027	0.025	0.028	0.027
70	0.16	0.11			0.047	0.044	0.052	0.050
80		0.15	0.060	0.055	0.075	0.070		
90		0.19	0.056	0.070	0.11	0.10		
100	0.36	0.20	0.090	0.10	0.16	0.14	0.14	0.13
150				0.27				0.31
200		0.47		0.35	0.52	0.45		0.45
300								0.65
400				0.66		0.87		0.78
600								1.0

TABLE II. Model parameters used in comparing Bohdansky's and Yamamura and Tawara's sputtering yield predictions with near-threshold experimental data. Reference surface binding energies U_s and fitting parameters $Q(Z_2)$, $W(Z_2)$, and $s(Z_2)$ used to evaluate Yamamura and Tawara's expression are taken from Ref. 8. U_s values from (Ref. 8) are also used to evaluate Bohdansky's expression.

				Bohdansky[a]	Yamamura and Tawara[b]			
Target	A	U_s		E_{th}	Q	W	s	E_{th}
Si	0.70	4.63	Ref.	43	0.66	2.32	2.5	32
			New-fit	20	1.3	2.32	2.5	18
Mo	2.53	6.82	Ref.	38	0.85	2.39	2.8	28
			New-fit	33	1	2.39	2.5	33
Ru	2.40	6.74	Ref.	37	1.31	2.36	2.5	27
			New-fit	33	1.31	2.36	2.5	33

[a]Reference 7.
[b]Reference 8.

were made while optimizing E_{th} for Bohdansky's formula and Q, W, s, and E_{th} for Yamamura's formula. The results together with the best-fit curves and the best-fit parameters are shown in Fig. 4 and listed in Table II, respectively. As a reference, Table II also lists the original parameters that were used to calculate the curves shown in Fig. 3. When comparing the parameters from Bohdansky and Yamamura–Tawara with those obtained in this work, especially for Si, a large discrepancy is found in the sputter threshold E_{th}. We pose that the thresholds presented here are more accurate than those presented in Refs. 7 and 8 due to the extension of experimental data to the threshold region. Although data on the heavy elements Mo and Ru are well reproduced by the equations assuming only a different E_{th}, a large discrepancy remains for the lighter element Si, where experimental sputtering yields are generally much higher than predicted ones. Only by adjusting the value of Q, good agreement with the experimental data can be achieved. An increased sputtering yield efficiency for Si may also be recognized in Ref. 17, although it was not remarked upon at the time.

Further improvement in the modeling of sputtering yields near the threshold energy has been carried out using a Monte Carlo program TRIM.SP.[18,19] However, it is still difficult to find physical basis to generalize the calculated yields at such low energy due to the multiple scattering processes. The accurate experimental data and methods presented in this work may be used as a basis for an improved theoretical description of physical sputtering at energies close to the sputtering threshold. In addition, these experiments, together with a high flux plasma and ion beam facility [Pilot-PSI (Ref. 20)] will enable accelerated lifetime experiments at conditions relevant to plasma-facing optics used in EUV lithography.

VI. CONCLUSION

Sputtering yields of Ru, Mo, and Si at low incident ion energies have been measured by means of *in situ* weight-loss measurements using a QCM and FC, as well as a thickness-decrease measurement using GIXR. The analysis and comparisons show that these experimental results on the sputtering yield at "near-threshold energy" are between the predictions of Bohdansky's and Yamamura and Tawara's calculations with their empirical parameters. In order to interpret the experimental data given in this paper, improved fit parameters are provided and discussed. The data presented here can be used as a basis for further theoretical studies on near-threshold sputtering and enables lifetime studies of plasma-facing optics such as those used in EUV lithography.

ACKNOWLEDGMENTS

The work is part of the ACHieVE and EAGLE programmes carried out under the auspices of ASML (Veldhoven, The Netherlands). Acknowledgments are due to the FOM Industrial Partnership Programme I10 (XMO), which is carried out under contract with the "Stichting voor Fundamenteel Onderzoek der Materie (FOM)," being financially supported by the "Nederlandse Organisatie voor Wetenschappelijk Onderzoek (NWO)" and SenterNovem.

[1]H. Meiling, H. Meijer, V. Banine, R. Moors, R. Groeneveld, H.-J. Voorma, U. Mickan, B. Wolschrijn, B. Mertens, G. van Baars, P. Kürz, and N. Harned, Proc. SPIE **6151**, 615108 (2006).
[2]S. N. Srivastava, K. C. Thompson, E. L. Antonsen, H. Qiu, J. B. Spencer, D. Papke, and D. N. Ruzic, J. Appl. Phys. **102**, 023301 (2007).
[3]M. H. L. van der Velden, W. J. M. Brok, J. J. A. M. Van der Mullen, and V. Banine, J. Appl. Phys. **100**, 073303 (2006).
[4]M. H. L. van der Velden, W. J. M. Brok, J. J. A. M. van der Mullen, W. J. Goedheer, and V. Banine, Phys. Rev. E **73**, 036406 (2006).
[5]R. C. Wieggers, W. J. Goedheer, M. R. Akdim, F. Bijkerk, and P. A. Zegeling, J. Appl. Phys. **103**, 013308 (2008).
[6]V. S. Smentkowski, Prog. Surf. Sci. **64**, 1 (2000); P. C. Zalm, Surf. Interface Anal. **11**, 1 (1988).
[7]J. Bohdansky, Nucl. Instrum. Methods Phys. Res. B **2**, 587 (1984).
[8]Y. Yamamura and H. Tawara, At. Data Nucl. Data Tables **62**, 149 (1996).
[9]W. Eckstein and R. Preuss, J. Nucl. Mater. **320**, 209 (2003).
[10]N. Laegreid and G. K. Wehner, J. Appl. Phys. **32**, 365 (1961).
[11]H. J. Voorma, E. Louis, F. Bijkerk, and S. Abdali, J. Appl. Phys. **82**, 1876 (1997).
[12]T. Tsarfatia, E. Zoethout, R. van de Kruijs, and F. Bijkerk (unpublished).
[13]R. D. Kolasinski, J. E. Polk, D. Goebel, and L. K. Johnson, J. Vac. Sci. Technol. A **25**, 236 (2007).
[14]D. L. Windt, Comput. Phys. **12**, 360 (1998).
[15]H. H. Andersen and H. L. Bay, in *Sputtering by Particle Bombardment I, Topics in Applied Physics*, edited by R. Behrisch (Springer, Berlin, 1981), Vol. 47.
[16]G. Sauerbrey, Z. Phys. **155**, 206 (1959).
[17]W. Eckstein, in *Sputtering by Particle Bombardment, Topics in Applied Physics*, edited by R. Behrisch and W. Eckstein (Springer, Berlin, 2007),

Vol. 110.
[18]W. Eckstein, J. Roth, W. Nagel, and R. Dohmen, J. Nucl. Mater. **328**, 55 (2004).
[19]W. Eckstein, C. Garciarosales, J. Roth, and J. Laszlo, Nucl. Instrum. Methods Phys. Res. B **83**, 95 (1993).
[20]G. J. van Rooij, V. P. Veremiyenko, W. J. Goedheer, B. de Groot, A. W. Kleyn, P. H. M. Smeets, T. W. Versloot, D. G. Whyte, R. Engeln, D. C. Schram, and N. J. L. Cardozo, Appl. Phys. Lett. **90**, 121501 (2007).